Fast and easy radiometric calibration method integration time insensitive for infrared thermography

Corentin Poissenot-Arrigoni *, Bertrand Marcon, Frédéric Rossi, Guillaume Fromentin

Arts et Metiers Institute of Technology, LaBoMaP, UBFC, HESAM, F-71250 Cluny, France

Keywords:
Infrared thermography
Integration time
Radiometric calibration
Pixel wise calibration

A B S T R A C T

The radiometric calibration of an infrared camera is a crucial and unavoidable step to obtain an accurate temperature measurement. The calibration does the link between the sensor digital levels and the actual radiometric temperature. Although this step is critical and necessary to obtain meaningful measurement, it is a complex and time-consuming procedure, which requires many experimental data acquisitions and an algorithm to process them. This article proposes a method based on the radiance data processing allowing an easily and quickly radiometric calibration. Thanks to the proposed method, an integration time insensitive radiometric calibration is obtained from only two different observed steady and homogeneous thermal conditions (using a black body or equivalent).

1. Introduction

The thermographic is more and more involved to measure the temperature of a scene, because it is a non-contact and a non-destructive measurement method, relatively easy to perform. Moreover, infrared cameras become more and more cheap and efficient. However, to obtain an accurate temperature, it is mandatory to take some precautions because this measurement method implies several sources of errors [1]. Firstly, the radiometric calibration, which is necessary to convert digital levels into radiometric temperatures, could create significant errors; among them, the main ones are: the imperfection of the black body source used during the data acquisitions (both in temperature and emissivity) [2], the procedure of non-uniformity correction (NUC) [3,4], or for example, the fitting error between the calibration curve and the experimental points cloud. Secondly, the good knowledge of the observed scene local emissivity is essential to convert radiometric temperatures into actual absolute temperatures. In addition, for a given material, it is important to mention that the viewed spectral emissivity of the observed scene depends at least of: the spectral range of the camera [5], the absolute temperature of the material [6], the surface preparation of the observed object (colour, roughness, reflectance, uniformity…) [7], and the incidence angle between the observed object and the camera lens [8]. Thirdly and less obvious than the other sources, the environment radiance could affect noticeably the temperature measurement as well [9].

Since the radiometric calibration is essential in the digital levels conversion into absolute temperatures, many studies are present in the literature. The two-point calibration method is a simple local method resulting in an excellent image quality and it requires only two experimental points (two different black body temperatures) for its implementation. However, this method is considered as valid only around an operating point (the two black body temperature ranging around that operating point), for a single integration time, a single ambient temperature, and it allows observing just low-contrasted scenes. At the opposite, the multi-points calibration is a global method, allowing to observe contrasted scenes. It is valid for discrete integration times and ambient temperatures, but the interpolation between the selected values are possible, including some strong approximations. Nevertheless, this method is complex and requires many experimental data resulting in being a time-consuming method to be correctly implemented [10,11]. Some studies, like that of Schweikert et al. [12] or Ochs et al. [13], propose to reduce the radiometric calibration errors by replacing the non-uniformity correction (NUC) by a pixel-wise calibration. Therefore, with this method, an independent calibration curve is obtained for each pixel of the sensor. In addition, Svensson et al. [14] and Le Saux and Doudard [3], compare the NUC calibration with the pixel-wise calibration; both demonstrate that the pixel-wise calibration seems to be more relevant than the NUC procedure to obtain an accurate radiometric calibration. Finally, Tremblay et al. [15,16] propose to work with the concept of digital level flow (being the digital level divided by the integration time to acquire the considered frame) rather than the actual

* Corresponding author.
E-mail address: corentin.poissenot@ensam.eu (C. Poissenot-Arrigoni).

https://doi.org/10.1016/j.infrared.2023.104741

Nomenclature

Rad	Radiance: [W.m^{-2}.sr^{-1}]
λ	Wavelength: [m]
ϵ	Emissivity: [–]
h = 6.6226176x10^{-34}	Planck constant: [J·s]
k = 1.380662x10^{-23}	Boltzmann constant: [J·K^{-1}]
c = 2.998x10^{8}	Celerity of light: [m·s^{-1}]
λ_1, λ_2	Spectral range of the sensor of the camera: [m, m]
NUC	Non-Uniformity Correction
n	Number of images by acquisition file: [–]
Num_{im}	Image number in an acquisition file: [–]
IT	Integration time: [μs]
T_{BBS}	Black body source temperature: [k]
T_{Env}	Environment temperature: [k]
X, Y	Coordinates of a pixel on the sensor matrix: [-, -]
$T_{Num\_im,\ X,\ Y}$	Absolute temperature of a pixel of an image: [k]
$DL_{Num\_im,\ X,\ Y}$	Digital level of a pixel of an image: [counts]
Mflow	Mean of the digital level flow: [counts.μs^{-1}]
$\overline{\overline{A}}$ when considering the full sensor	Slope coefficient of the calibration curve: A when considering only one pixel; [W·μs·m^{-2}·counts^{-1}·sr^{-1}]
$\overline{\overline{B}}$ when considering the full sensor	Offset coefficient of the calibration curve: B when considering only one pixel; [W·m^{-2}·sr^{-1}]

digital levels, in view to obtain a radiometric calibration insensitive to the integration times. It is a global method combining both advantages of allowing to observe contrasted scenes and to reach a very accurate temperature measurement. In addition, it is valid for any integration times and ambient temperatures. However, this technic implies to use many experimental points to obtain the calibration curve as it was the case for the above-mentioned multi-points calibration ([10,11]).

To resume, the radiometric calibration is an essential step, impossible to discard, to obtain accurate absolute temperature measurements, but it is a complex and time-consuming procedure. The aim of this study is to present an original method enabling an accurate radiometric calibration being integration time insensitive, with an easy and fast experimental procedure. According to the presented state of the art, the novelty of the proposed method is to obtain a global radiometric time insensitive calibration from only two different temperature measurements using a black body source, without constraints on the integration time. Therefore, this calibration method results in a fast and easy experimental procedure. Basically, this new method gathers together all advantages of the already existing calibration methods into a single one. Firstly, the hypothesis involved in this approach will be exposed before describing the steps of its implementation. Then the demonstration of the great accuracy of the method will be assessed through observations of a black body by scanning all the possible integration times and temperature observable range with a certain camera/filter configuration which is totally possible to generalize to other configurations.

2. Description of the calibration method

2.1 Hypothesis

At the scale of this study, it has been considered that the atmospheric transmission has a negligible impact on the temperature measurement, compared to others sources of errors. Based on works of Monchau [17] and Pajani [18], in the experimental conditions of this study, this hypothesis involves an error of the measured radiometric temperature lower than 1 K. The developed method allows to obtain an infrared camera calibration insensitive to integration times (IT) and assumes that the radiance of the observed scene is proportional to the digital level flow (DL/IT) in the sensor output of the infrared camera. Then, Eq. (3) is proposed for modelling observed radiance:

$$Observedradiance = \overline{\overline{A}} \times \frac{DL}{IT} + \overline{\overline{B}}\left(\overline{\overline{A}}, \overline{\overline{B}}\right) \in \mathbb{R}^2 \tag{1}$$

where $\overline{\overline{A}}$ and $\overline{\overline{B}}$ are the constants of the linear approximation equation. In view to confirm this hypothesis, an Ametek Landcal P1200B black body source, which has an indicated emissivity of 0.998, was observed by a Telops MS-M3K infrared camera at different conditions, with a 25 mm focal lens (Telops, 25 mm f/2.3 MWIR) and a frame rate of 60 Hz. This camera has a cooled InSb (Indium Antimonide) sensor, with a full frame resolution of 320 × 256 pixels^2, a pitch of 30 × 30 μm^2, and an average Noise Equivalent Temperature Difference (NETD) of 25 mK. In addition, the native spectral range of the sensor is 1.50–5.50 μm. However, a broadband filter was positioned in front of the sensor, reducing the spectral range to 3.11–5.50 μm, in view to work in the mid-wave infrared spectral range (the spectral range typical of gases being not of interest in the current application). The experimental set-up is shown in Fig. 1.

Given the fact that the approach works directly in radiance rather than in temperature, it is necessary to link the black body temperature with its radiance. For this, the usual Planck's law expressed for a solid angle, shown in Eq. (2) has been used.

$$Rad(T_{BBS}) = \int_{\lambda_1}^{\lambda_2} \frac{2\,h\,c^2\,\lambda^{-5}}{\exp\left(\frac{h\,c}{\lambda\,k\,T_{BBS}}\right) - 1}\,d\lambda\left[W.m^{-2}.sr^{-1}\right] \tag{2}$$

with *Rad* the observed radiance of the black body at the temperature set T_{BBS}, λ the considered wavelength, h = 6.6226176 × 10^{-34} J.s the Planck's constant, c = 2.998 × 10^8 m.s^{-1} the light celerity, and k = 1.380662 × 10^{-23} J.K^{-1} the Boltzmann's constant. In all the study, the integration interval of the Planck's law corresponds to the spectral range of the camera sensor equipped with a so-called broad band filter as mentioned before (λ_1 = 3.11 μm and λ_2 = 5.50 μm). The integral was calculated numerically by the trapeze method with a step of 3.9 × 10^{-4} μm, which discretizes the spectral band in 1000 elements with a considered low residue.

Table 1 summarises the experimental conditions studied and results for the pixel located at the coordinates (160,128), which corresponds to the pixel at the centre of the sensor. It is important to note that the total range of observable temperatures available with this camera configuration (full optical path: sensor, broad band filter, and lens) was covered. On the other hand, for each temperature, the maximum and minimum integration times corresponds respectively to the integration time avoiding any pixel saturation (over the whole sensor) and the one allowing for at least a pixel filling of 5%. Furthermore, the behaviour of all pixels was analysed, but in this article, the results of only one representative pixel (the central one arbitrarily) is presented for the sake of brevity.

Fig. 2 depicts the evolution of the observed radiance with the digital level flow of the central pixel (160,128), and the equations are the results of linear regressions of the measured points calculated by the least square method. In the most unfavorable case, which corresponds to the maximum integration times presented on the Fig. 2 (a), a linear trend residue of 0.9997 has been observed allowing to consider that the digital level flows (DL/IT) measured by the sensor pixels react linearly relative to the observed radiance. This point had being already figured out by [13] who verified this hypothesis for an InSb sensor. In addition, [19,20] show that for others sensor technologies, digital levels reacts linearley toward the integration time. Therefore, it seems that this hypotesis is valid for an InSb sensor, and could be extended for some others sensor technologies too.

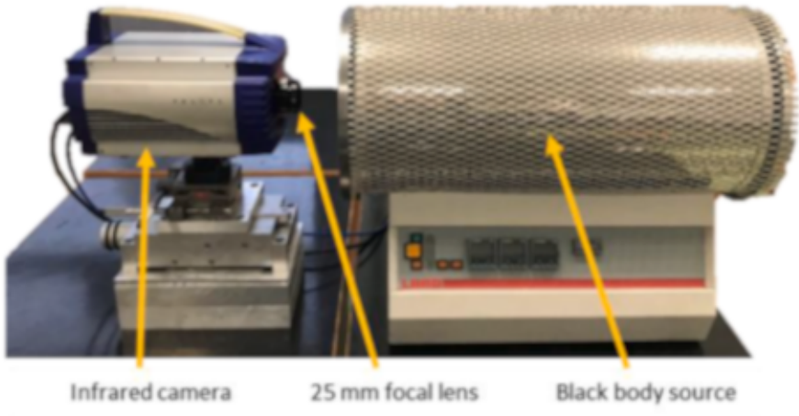

Fig. 1. Experimental set-up of the black body source observation.

Table 1
Experimental conditions and results for the analysis of the behavior of the sensor towards the radiance.

	Experimental conditions T_{BBS}; IT	Black body temperature [°C] *	Black body radiance [W.m^{-2}.sr^{-1}] **	IT [μs]	DL [counts]	DL.IT^{-1} [counts.μs^{-1}]
Maximum integration times	50 °C; 120 μs	50	7.1093	120.00	34,836	290.3
	75 °C; 80 μs	75	14.0683	80.04	37,876	473.2
	100 °C; 40 μs	100	25.5808	40.00	30,465	761.6
	125 °C; 20 μs	125	43.3996	20.04	23,783	1186.7
	150 °C; 20 μs	150	69.5105	20.04	36,498	1821.2
	175 °C; 10 μs	175	106.0699	9.96	26,512	2661.8
Minimum integration time	50 °C; 10 μs	50	7.1093	9.96	2848	285.9
	75 °C; 10 μs	75	14.0683	9.96	4671	468.9
	100 °C; 10 μs	100	25.5808	9.96	7484	751.4
	125 °C; 10 μs	125	43.3996	9.96	11,761	1180.8
	150 °C; 10 μs	150	69.5105	9.96	17,907	1797.9
	175 °C; 10 μs	175	106.0699	9.96	26,512	2661.8

*The black body temperature corresponds to the temperature set in the black body source during experimental data acquisition.
**The radiance of each condition is calculated using the Planck's law expressed for a solid angle (integration method explained in Section 2.1), from the black body temperature thanks to the Eq. (2).

2.2. *Implementation of the calibration method*

2.2.1. *Determination of pixel by pixel calibration matrixes*

After the linear dependency of the radiance toward the digital level flow has been proven in the previous subsection, it is possible to obtain an infrared camera radiometric calibration insensitive to the integration time; and so, from only two different acquisition data of a black body source at two different temperatures and without constraints regarding the integration time (as long as the sensor has no underexposed or saturated pixel). Indeed, given the calibration trend is linear, two experimental points are sufficient to calculate its coefficients (the slope and the offset coefficients). To do so, the following procedure is suggested:

Firstly, experimental data are required to obtain a radiometric calibration. For this, a black body source must be observed at different temperatures by the infrared camera (Fig. 1 shows an example of a possible experimental setup).

Secondly, it is necessary to convert the different temperatures of the observed black body source in radiance. For this, the Planck's law (presented in the Eq. (2)) is integrated within the spectral range of the whole optical path and sensor (as explained in Section 2.1).

Thirdly, the digital levels flow of the data acquisition must be determined. For this, digital levels are sorted by integration time. In addition, in view to reduce the calibration errors due to measuring uncertainties, it could be beneficial to calculate a mean of the digital levels flow based on the acquisition data of several consecutive images. In Section 3, it will be estimated that a measure based on a set of 125 images is acceptable to ensure a repeatability below 0.01 %. Finally, given that the procedure of non-uniformity correction (NUC) induces approximations, it has been decided at the scale of this study, to realise an independent calibration for each pixel. Therefore, it is necessary to calculate the digital levels flow for each pixel of the sensor independently, as described in the following Eq. (3) for given condition (Ci).

$$Mf_{flow}(Ci)_{X,Y} = \frac{1}{n} \times \sum_{Num_{ac}=1}^{n} \frac{DL_{Num_{ac},X,Y}}{IT} \left[counts.\mu s^{-1}\right] \quad (3)$$

Afterward, from the radiance (obtained thanks to the Eq. (2)) and the mean of the digital levels flows for two different conditions (referred as C1 and C2), obtained from the Eq. (3), coefficients of the linear trend (slope coefficient matrix $\overline{\overline{A}}$ and offset matrix $\overline{\overline{B}}$) could be calculated thanks to Eqs. (4) and (5):

$$A_{X,Y} = \frac{Rad(C1) - Rad(C2)}{Mflow(C1)_{X,Y} - Mflow(C2)_{X,Y}} \left[W.\mu s.m^{-2}.counts^{-1}.sr^{-1}.\right] \quad (4)$$

$$B_{X,Y} = \frac{Mflow(C1)_{X,Y} \times Rad(C2) - Mflow(C2)_{X,Y} \times Rad(C1)}{Mflow(C1)_{X,Y} - Mflow(C2)_{X,Y}} \left[W.m^{-2}.sr^{-1}\right] \quad (5)$$

Finally, the coefficients of the integration time insensitive radiometric calibration are obtained from only two different experimental conditions. Fig. 3 summarizes the algorithm to compute the two matrixes of calibration: $\overline{\overline{A}}$ and $\overline{\overline{B}}$ for each pixel of the sensor having both the dimensions of the sensor in pixels. With the Telops MS-M3K used in the present work as case study of the calibration method, the matrix $\overline{\overline{A}}$ and $\overline{\overline{B}}$

have both the dimension (320,256).

2.2.2. Conversion of digital levels pictures to radiometric temperatures

Once the linear trend coefficients of the calibration determined, it is possible to convert an image coded in digital levels into absolute temperatures following the following procedure:

Firstly, digital levels must be converted into radiances by transforming the measured digital levels from the sensor into a flow of digital levels and dividing them by the integration time used to acquire the considered frame. Then, the radiances are obtained directly by applying the calibration coefficients using Eq. (6):

$$Rad(Num_{bw})_{X,Y} = A_{X,Y} \times \frac{DL_{Num_{bw},X,Y}}{IT} + B_{X,Y}\left[W.m^2.sr^{-1}\right] \quad (6)$$

Secondly, based on the results of Li et al. [21], the Eq. (7) links the radiance of the observed scene to different radiation sources, in experimental conditions of this study is:

$$Rad(Num_{bw})_{X,Y} = \epsilon_{\lambda_1,\lambda_2} \times \int_{\lambda_{1(Num),Y}}^{\lambda_{2(Num),Y}} \frac{2\,h\,c^2\,\lambda^{-5}}{\exp\left(\frac{h\,c}{\lambda\,k\,T_{Num_{bw},X,Y}}\right) - 1} d\lambda + \left(1 - \epsilon_{\lambda_1,\lambda_2}\right) \times \int_{\lambda_{1(Num),Y}}^{\lambda_{2(Num),Y}} \frac{2\,h\,c^2\,\lambda^{-5}}{\exp\left(\frac{h\,c}{\lambda\,k\,T_{Env}}\right) - 1} d\lambda \left[W.m^2.sr^{-1}\right] \# \quad (7)$$

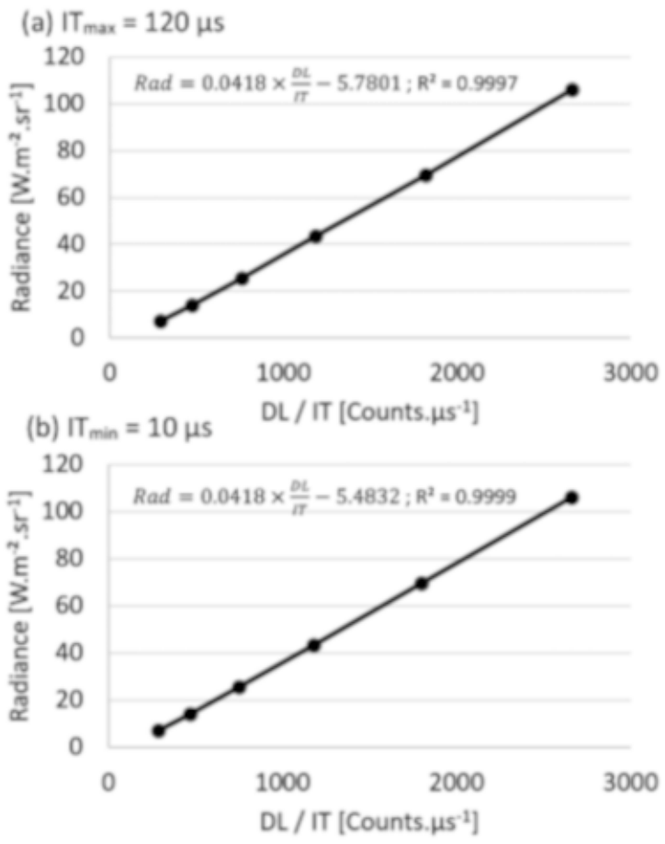

Fig. 2. Experimental response of the pixel (160,128) observed radiance with the digital level flow and their associated linear trends: (a) for the maximum integration times, and (b) the minimum integration times.

with $\epsilon_{\lambda_1,\lambda_2}(T,\theta,\varphi)$, the emissivity of the observed scene. It is not possible to invert directly the Eq. (8) because the Planck's integral has no analytical solution. Thus, to obtain a direct link between the observed radiance and the absolute temperature of the scene, it is necessary to calculate numerically the Planck's integral. This computation had been performed here in the same way than in Section 2.1. Fig. 4 summarizes that above described procedure allowing to convert digital levels images into absolute temperature ones.

3. Results and discussions

The objective of this part is to validate experimentally the calibration method presented previously. For this, an Ametek Landcal P1200B black body source was observed by a Telops MS-M3K infrared camera, with a 25 mm lens, as shown in Fig. 1. The experimental setup and characteristics of the black body source and the infrared camera are the same as mentioned in Section 2.1. In view to improve the measurement accuracy of the calibration method, it could be relevant to choose in input, the two measured temperatures as far away as possible, because it reduces the impact of measurement uncertainties on the calibration coefficients values. Moreover, given the calibration method is insensitive with the integration time, there are no specific setting to consider about this parameter (once again, as long as the sensor has no underexposed or saturated pixel). Therefore, it could be interesting for each condition to adapt the integration time in view to optimise the measurement quality. For this, two indicators, independent of the observed temperature, and the integration time have been used. The first is the pixel load; this criterion allows determining if the sensor had been over or underexposed during the exposition (integration time). It could be defined as the ratio of collected photons by the maximum capacity of photons before saturation of the considered quantic well (Eq. (8)). It is important to note that the maximum photons capacity of the sensor is considered in this study by the value just before the saturation of the first pixel on all

Algorithm 1: Identification of the calibration matrixes

Input: Camera data of the black body source observation

1: Open camera files: [DL, IT] = read camera data

2: Compute observed radiance C1 and C2: $\mathrm{Rad}(Ci) = \int_{\lambda_1}^{\lambda_2} \frac{2\,h\,c^2\,\lambda^{-5}}{\exp\left(\frac{h\,c}{\lambda\,k\,Ci}\right)-1}\,d\lambda$

3: Compute the digital levels flow C1 and C2: $\mathrm{Mflow(Ci)}_{X,Y} = \frac{1}{n} \times \sum_{Num_{im}=1}^{n} \frac{DL_{Num_{im},X,Y}}{IT}$

4: Compute the slope coefficient of the calibration curve: $A_{X,Y} = \frac{\mathrm{Rad(C1)} - \mathrm{Rad(C2)}}{\mathrm{Mflow(C1)}_{X,Y} - \mathrm{Mflow(C2)}_{X,Y}}$

5: Compute the offset coefficient: $B_{X,Y} = \frac{\mathrm{Mflow(C1)}_{X,Y} \times \mathrm{Rad(C2)} - \mathrm{Mflow(C2)}_{X,Y} \times \mathrm{Rad(C1)}}{\mathrm{Mflow(C1)}_{X,Y} - \mathrm{Mflow(C2)}_{X,Y}}$

Outputs: Matrix $\overline{A}$ and $\overline{B}$

Fig. 3. Algorithm to identify the calibration matrixes coefficients.

Algorithm 2: Conversion from digital levels to absolute temperatures

Inputs: Camera data of the observed scene, matrix $\overline{\overline{A}}$ and $\overline{\overline{B}}$ of Algorithm 1, emissivity of the observed scene

1: Setting inputs: [DL, IT] = read camera data
[$\overline{\overline{A}}$, $\overline{\overline{B}}$] = read matrix $\overline{\overline{A}}$ and $\overline{\overline{B}}$
$\epsilon_{\lambda_1,\lambda_2}$ = input emissivity of observed scene

2: Conversion from digital levels to radiance: $Rad(Num_{Im})_{X,Y} = A_{X,Y} \times \frac{DL_{Num_{Im}X,Y}}{IT} + B_{X,Y}$

3: Conversion from radiance to absolute temperature

$$Rad(Num_{Im})_{X,Y} = \epsilon_{\lambda_1,\lambda_2} \times \int_{\lambda_{1wn,f}}^{\lambda_{2wn,f}} \frac{2\,h\,c^2\,\lambda^{-5}}{\exp\left(\frac{h\,c}{\lambda\,k\,T_{Num_{Im}X,Y}}\right) - 1}\,d\lambda + \left(1 - \epsilon_{\lambda_1,\lambda_2}\right) \times \int_{\lambda_{1wn,f}}^{\lambda_{2wn,f}} \frac{2\,h\,c^2\,\lambda^{-5}}{\exp\left(\frac{h\,c}{\lambda\,k\,T_{Env}}\right) - 1}\,d\lambda$$

Output: Matrix of absolute temperature $T_{Num_{Im}X,Y}$

Fig. 4. Algorithm of conversion from digital levels to absolute temperatures.

the sensor.

$$Pixelwell - filling = \frac{\text{Collected photons}}{\text{Maximum photons capacity}} \times 100[\%] \quad (8)$$

The second is a measurement repeatability criterion. By considering that the black body source gives a spatial and temporal homogeneous temperature, in theory, each measure take in same conditions should give exactly the same results. Thus, the measurement repeatability criterion could be evaluated for each pixel by considering the relative deviation between the pictures with the maximum measured digital levels and that with the minimum measured digital levels, captured on a set (Eq. (9)). In practice, each set contains 125 frames captured at a frequency of 60 Hz and the field of view is about one square centimetre. Then, it seems reasonable to consider that the black body source gives homogeneous temperature.

$$Repetability = \frac{DL_{maximum} - DL_{minimum}}{DL_{maximum}} \times 100[\%] \quad (9)$$

Fig. 5 (a) presents the design of experiment realised in this study (for each condition, the mean pixel load of the sensor has been indicated in the table). It is important to note that the minimum and maximum temperatures correspond to extremes observable temperatures by the camera in these experimental conditions. The design of experiment is made up of 29 different conditions and the sensor has a resolution of 320×256 pixel^2. Given each pixel has an independent calibration in the present method, this design of experiment allows to assess the approach on more than 2.3 million results. Fig. 5 (b) presents the evolution of the mean of the digital level flow and the repeatability criterions on the entire sensor, in function of the well-filling, for a constant radiometric temperature of 50 °C.

Given that it has been shown in the part 2.1 that the flux of digital levels reacts linearly toward the radiance, for a constant observed temperature, this flux should not be affected by the variation of the integration time (and then the pixel load). However, for low and high well filling, the digital levels flux is affected by the variation of integration time. In addition, in regions where the sensor reacts not linearly with the integration time, the repeatability is significantly deteriorated.

Table 2
Input parameters in the algorithm of matrix calibration and of conversion of digital levels into temperatures.

Parameters	Values
Spectral range of the sensor of the camera: λ_1- λ_2	3.11–5.50 [µm]
Environment temperature: T_{Env}	20.00 [°C] or 293.15 [K]
Emissivity: ϵ	0.998 [-] *
Wavelength discretization for the calculation of the Planck's integral	3.90x10^{-4} [µm]
Temperature discretization for the calculation of the Planck's integral	0.001 [K]

* The input emissivity corresponds to the emissivity of the black body source provided in its calibration certificate.

		Black body setting temperatures [°C]					
		50	75	100	125	150	175
		Sensor average pixels well-filling [%]					
IT [µs]	1	0.1	0.3	0.9	1.5	2.3	3.4
	5	3.7	5.5	8.8	13.7	20.9	30.9
	10	6.7	11.1	17.7	27.7	42.3	62.5
	20	13.6	22.4	38.0	56.2	86.0	100
	40	27.3	44.9	71.9	100	100	100
	60	41.0	67.4	100	100	100	100
	80	54.7	90.0	100	100	100	100
	100	68.3	100	100	100	100	100
	120	82.1	100	100	100	100	100
	140	98.5	100	100	100	100	100
	160	100	100	100	100	100	100

(a)

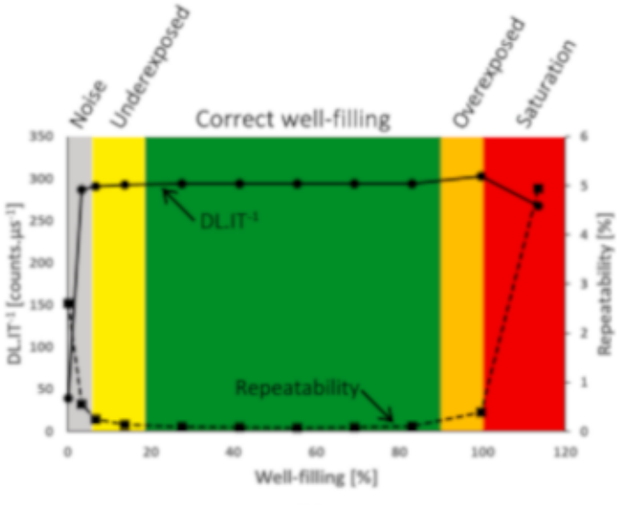

(b)

Fig. 5. (a) Data experiment setting with the average sensor pixels well-filling for each condition, and (b) corresponding thresholds (associated with a colorbar) to determine the optimized conditioned of integration times for the observed black body temperature (example given here for 50 °C).

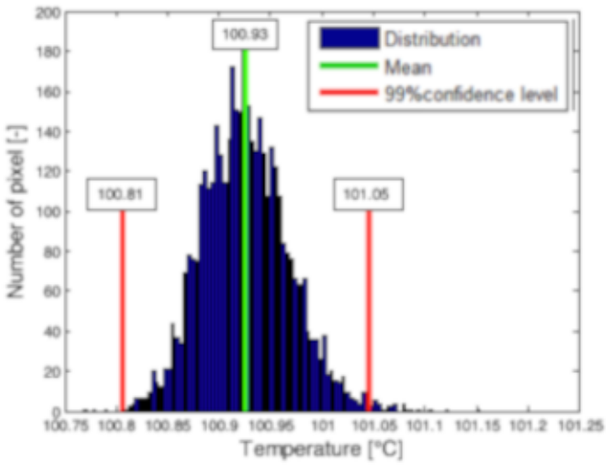

Fig. 6. Pixels distribution of the radiometric temperatures for the condition {100 °C; 20 µs} where the maximum temperature discrepancy compared to the black body setting is observed among the design of experiments exposed in Table 2.

For conditions with low well-filling (pixels under-exposed), the measurement uncertainty increases because of the dominance of the noise. Therefore, to ensure that the measure is taken in the operating point of the sensor, it seems relevant to choose a well-filling minimising the repeatability criterion. Based on the wide design of experiment presented in the Table 2, a colorbar associated to the well-filling, which indicates the measurement quality, is proposed in Fig. 5(b). A correct well-filling is considered when the repeatability criterion is lower than 0.01% and the relative fluctuation of the digital levels flow between two consecutive experimental points is lower than 0.2%. For the data processing, parameters presented in the Table 2 were input in the algorithm of the calibration matrixes (method described in Section 2.2.1) and the conversion algorithm of digital levels into absolute temperatures (method described in Section 2.2.2).

Firstly, two conditions must be chosen to obtain the calibration coefficients ($\overline{\overline{A}}$ and $\overline{\overline{B}}$). In view to obtain the bests results with this calibration method, it seems that it is appropriate to choose experimental temperatures close to the limit of the observable temperatures of the camera in its setting conditions. Thus, it has been chosen to take 50 °C and 175 °C. Moreover, one of the advantages of this calibration method is that it is insensitive to integration times (point already discussed before). Therefore, to ensure pixel well-fillings of approximately 80%, it seems relevant to choose an integration time of 120 µs for the measure (black body setting) at 50 °C, and 10 µs for the measure at 175 °C. After obtaining the calibration matrixes coefficients, the digital levels provided by the sensor of the scene observed under all conditions presented in the Table 2 are converted into temperatures thanks to the method presented in the previous section. Finally, the worst result, temperature error compared to the black body one, has been obtained for the condition {100 °C; 20 µs} and for the pixel of sensor coordinates (15,25). Fig. 6 presents the radiometric temperatures distribution calculated for all pixels of the sensor and for this last sensor setting {100 °C; 20 µs}.

From Fig. 6, the absolute error for the worst pixel is 1.16 °C. However, the mean error of all pixels of the picture is 0.93 °C and 99% of the results are contained in a temperature range of 0.24 °C, corresponding to the gap 100.93 ± 0.12 °C. In order to reduce the maximum error obtained with the proposed method, it could be relevant to obtain the calibration matrixes coefficients, not from only two measuring points, but from more measuring points and to use the least square method to calculate the linear trend equation allowing scattering the errors in the whole temperature domain, which could improve the global accuracy. In view to study the influence of the number of points used to determine the calibration coefficients on the calibration accuracy, it has been decided to independently identify them from 2 to 6 experimental points (2 being the above exposed results), and to analyze the results on the

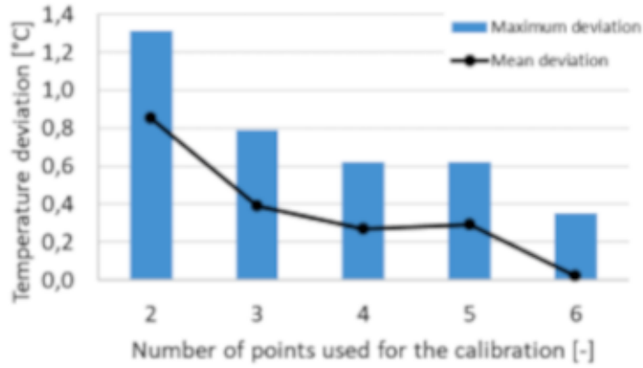

Fig. 7. Influence of the number of calibration points used for the calibration on the deviation between the black body temperature and the temperatures measured.

Table 3
Studied conditions and results of the influence of the number of points used for the calibration on the deviation between the black body and the infrared camera temperatures.

Number of calibration points	Conditions	Maximum deviation [°C]*	Mean deviation [°C]	99% confidence interval [°C]
2	50 °C; 40 µs 150 °C; 10 µs	1.16	0.93	0.24
3	50 °C; 40 µs 75 °C; 20 µs 150 °C; 10 µs	0.90	0.70	0.22
4	50 °C; 40 µs 75 °C; 20 µs 125 °C; 20 µs 150 °C; 10 µs	0.81	0.64	0.21
5	50 °C; 40 µs 75 °C; 20 µs 125 °C; 20 µs 150 °C; 10 µs 175 °C; 10 µs	0.84	0.65	0.22
6	50 °C; 40 µs 75 °C; 20 µs 100 °C; 20 µs 125 °C; 20 µs 150 °C; 10 µs 175 °C; 10 µs	0.54	0.40	0.19

* Maximum deviation between the black body and the camera temperature.

Table 4
Qualitative comparison of different radiometric calibration methods.

Calibration method	2-points	Multi-points	Tremblay and al. [14]	Presented here
Calibration type	Local	Global	Global	Global
Complexity	Low	Moderate to high	Moderate	Low
Implementation time	Low	High	High	Low
Accuracy	High	Differ from interpolation	High	Acceptable
Observable scenes	Low contrast	All	All	All
Integration time	Single	Discrete + interpolation	All	All

condition leading to the worst results: the condition {100 °C; 20 μs}, see Table 3.

In addition, Fig. 7 presents the influence of the number of reference points used for the calibration towards the temperature deviation of the black body temperature compared to the calculated temperature ones converted.

From Table 4, the condition with 6 experimental points for the calibration implementation is peculiar, because the condition {100 °C; 20 μs} (identified as the one providing the worse results) is included in this calibration. Therefore, it seems logical that the maximum and the minimum deviation are significantly reduced for this condition. Then, passing from 2 to 5 points for the calibration, the 99% confidence interval reduces only from 0.24 to 0.22 °C. Therefore, the number of calibration points seems to have a negligible influence on the 99% confidence interval. To resume, under those experimental conditions, it would appear that the use of 4 calibration points is the best trade-off between the accuracy and the experimental data necessary, reaching a maximum deviation of 0.81 °C and a mean deviation of 0.64 °C. Therefore, the calibration obtained from 4 experimental points allows to decrease the maximum and the mean deviation by about 30% compared to the calibration implemented with only 2 experimental points.

The proposed method allows obtaining a radiometric calibration insensitive to the integration times from only two measuring points. It seems that an accurate multi-points calibration or the calibration developed by Tremblay et al. [14] could allow obtaining a better accuracy than the proposed method. Indeed, the calibration method developed by Tremblay et al. [14] gives a measuring accuracy of 0.4 °C and a mean error of 0.2 °C, while the proposed method provides a measuring error of 1.16 °C and a mean error of 0.92 °C. Nonetheless, the maximum radiometric error of 0.4 °C in the study of Tremblay et al. [14] is obtained for a point used to obtain the calibration curve, which automatically reduces the error compared to a point between two conditions used to obtain the calibration curve. In addition, the presented study was not realized in laboratory conditions: the environment radiance, the humidity and the deficiencies of the black body source were not controlled.

Although, the method of Tremblay et al. [14] or a classic multi-points calibration method seem to be more accurate than the proposed method, those last are very time consuming and quite complex to implementation, whereas the proposed method is really very fast and simple. Furthermore, given the proposed method works from the radiance and not from the radiometric temperature, emissivity correction is more straightforward than classic method. Indeed, in the Planck's law, the absolute temperature is link to the radiance and not to the radiometric temperature.

At the end, the proposed method is not optimized in accuracy compared to others methods available in the literature. Nevertheless, it consists in an easy and fast radiometric calibration insensitive to the integration time with a rather acceptable low radiometric error.

4. Conclusions

This study proposes a new method to implement a radiometric calibration for thermography imaging. This method is based on the finding that the digital level flow of the InSb sensor reacts linearly with the radiance. Thereby, it is possible to obtain a calibration insensitive with the integration times; which simplifies significantly the use of such cameras. In addition, given the calibration curve is a straight-line (far from the sensor limits), only two temperatures measurement on a black body source, without constraints on the integration time, are necessary to access a good global accuracy calibration. The strong points of this method are:

- The proposed method is insensitive with the integration time, then it is possible to observe all scenes from a unique calibration block with optimized pixel fillings,
- This method allows a fast and easy implementation, because it is based on only two experimental conditions at different temperatures. Therefore, it is efficient in a time-consuming point of view,
- Given it is based on radiance, the conversion from radiometric to absolute temperature by the Planck's law is simplified.

Nevertheless, the proposed method is less accurate and a vagueness in the input data files led to a higher error than a multi-points calibration, because it is based on only two input data acquisition files. Then, this method globally simplifies the procedure of temperature measurement by the infrared thermography method. The Table 4 summarizes qualitatively the advantages of the different calibration methods with the one presented here.

To improve this study, it could be interesting to consider the atmospheric transmission. Moreover, a procedure of bad pixel replacement could be implemented in view to delete singulars behaviors of a few pixels which strongly impact the global accuracy when focusing on the maximum errors.

Declaration of Competing Interest

The authors declare that they have no known competing financial interests or personal relationships that could have appeared to influence the work reported in this paper.

Data availability

Data will be made available on request.

Acknowledgements

The authors would like to thank PR. G. Germain from Arts et Metiers Institute of Technology, LAMPA for his technical support and the Telops company for their advice and useful comments on this work.

References

[1] Y. He, Y. Fan, Y. Li, L. Chen, Analysis of multi-factor on measurement improvement of an infrared imager in low-temperature environments, Infrared Phys. Technol. 116 (2021), 103813, https://doi.org/10.1016/j.infrared.2021.103813.
[2] Y. Té, P. Jeseck, I. Pépin, C. Camy-Peyret, A method to retrieve blackbody temperature errors in the two points radiometric calibration, Infrared Phys. Technol. 52 (5) (2009) 187–192, https://doi.org/10.1016/j.infrared.2009.07.003.
[3] V. Le Saux, C. Doudard, Proposition of a compensated pixelwise calibration for photonic infrared cameras and comparison to classic calibration procedures: Case

of thermoelastic stress analysis, Infrared Phys. Technol. 80 (2017) 83–92, https://doi.org/10.1016/j.infrared.2016.11.008.
[4] J. Hu, Z. Xu, Q. Wan, Non-uniformity correction of infrared focal plane array in point target surveillance systems, Infrared Phys. Technol. 66 (2014) 56–69, https://doi.org/10.1016/j.infrared.2014.05.012.
[5] L. González-Fernández, L. del Campo, R.B. Pérez-Sáez, M.J. Tello, Normal spectral emittance of Inconel 718 aeronautical alloy coated with yttria stabilized zirconia films, J. Alloy. Compd. 513 (2012) 101–106, https://doi.org/10.1016/j.jallcom.2011.09.097.
[6] C.-D. Wen, I. Mudawar, Emissivity characteristics of polished aluminum alloy surfaces and assessment of multispectral radiation thermometry (MRT) emissivity models, Int. J. Heat Mass Transf. 48 (2005) 1316–1329, https://doi.org/10.1016/j.ijheatmasstransfer.2004.10.003.
[7] B.P. Keller, S.E. Nelson, K.L. Walton, T.K. Ghosh, R.V. Tompson, S.K. Loyalka, Total hemispherical emissivity of Inconel 718, Nucl. Eng. Des. 287 (2015) 11–18, https://doi.org/10.1016/j.nucengdes.2015.02.018.
[8] L. del Campo, R.B. Pérez-Sáez, L. González-Fernández, X. Esquisabel, I. Fernández, P. González-Martín, M.J. Tello, Emissivity measurements on aeronautical alloys, J. Alloy. Compd. 489 (2) (2010) 482–487, https://doi.org/10.1016/j.jallcom.2009.09.091.
[9] I. Fernández-Cuevas, J.C. Bouzas Marins, J. Arnáiz Lastras, P.M. Gómez Carmona, S. Piñonosa Cano, M.Á. García-Concepción, M. Sillero-Quintana, Classification of factors influencing the use of infrared thermography in humans: a review, Infrared Phys. Technol. 71 (2015) 28–55, https://doi.org/10.1016/j.infrared.2015.02.007.
[10] M. Sheng, J. Xie, Z. Fu, Calibration-based NUC method in real-time based on IRFPA, Phys. Proc. 22 (2011) 372–380, https://doi.org/10.1016/j.phpro.2011.11.058.
[11] F. Marcotte, P. Tremblay, V. Farley, Infrared camera NUC and calibration: comparison of advanced methods, in: Infrared Imaging Systems: Design, Analysis, Modeling, and Testing XXIV. Presented at the Infrared Imaging Systems: Design, Analysis, Modeling, and Testing XXIV, International Society for Optics and Photonics, 2013, p. 870603. 10.1117/12.2016265.
[12] K. Schweikert, A. Sielaff, P. Stephan, Pixel-wise in situ calibration method for high accuracy infrared thermography of moving targets, Infrared Phys. Technol. 118 (2021), 103862, https://doi.org/10.1016/j.infrared.2021.103862.
[13] M. Ochs, A. Schulz, H.-J. Bauer, High dynamic range infrared thermography by pixelwise radiometric self calibration, Infrared Phys. Technol. 53 (2010) 112–119, https://doi.org/10.1016/j.infrared.2009.10.002.
[14] T. Svensson, H. Larsson, J. Eriksson, Radiometric uncertainty of radiance measured with infrared cameras under variable ambient conditions, in: Bodermann, B., Frenner, K., Silver, R.M. (Eds.), Presented at the SPIE Optical Metrology, Munich, Germany, 2015, p. 95260E. 10.1117/12.2184861.
[15] P. Tremblay, L. Belhumeur, M. Chamberland, A. Villemaire, Radiometric calibration method for infrared detectors, USA Patent US20120239330A1 (2012) 35.
[16] Tremblay, P., Belhumeur, L., Chamberland, M., Villemaire, A., Dubois, P., Marcotte, F., Belzile, C., Farley, V., Lagueux, P., 2010. Pixel-wise real-time advanced calibration method for thermal infrared cameras, in: Infrared Imaging Systems: Design, Analysis, Modeling, and Testing XXI. Presented at the Infrared Imaging Systems: Design, Analysis, Modeling, and Testing XXI, SPIE, 325–335. 10.1117/12.850560.
[17] Monchau, J.-P., 2013. Mesure d'émissivité pour la thermographie infrarouge appliquée au diagnostic quantitatif des structures, PhD thesis, Université Paris-Est, Paris, France. p. 136. (French). tel-00952076.
[18] Pajani, D., 2013. Thermographie - Principes et mesure. Contrôle non destructif. Techniques de l'ingénieur (Eds.), r2740, Saint-Denis, France, p. 18. 10.51257/a-v2-r2740.
[19] W.F. Hoffmann, P.M. Hinz, D. Defrère, J.M. Leisenring, A.J. Skemer, P.A. Arbo, M. Montoya, B. Mennesson, Operation and performance of the mid-infrared camera, NOMIC, on the Large Binocular Telescope, in: Presented at the Ground-based and Airborne Instrumentation for Astronomy V, 2014, pp. 622–630, https://doi.org/10.1117/12.2057252.
[20] D. Ives, G. Finger, G. Jakob, S. Eschbaumer, L. Mehrgan, M. Meyer, J. Steigmeier, AQUARIUS, the next generation mid-IR detector for ground-based astronomy, in: Holland, A.D., Beletic, J.W. (Eds.), Presented at the SPIE Astronomical Telescopes + Instrumentation, Amsterdam, Netherlands, 2012, p. 845312. 10.1117/12.925844.
[21] D. Li, C. Feng, S. Gao, K. Daniel, L. Chen, Effect of pyrometer type and wavelength selection on temperature measurement errors for turbine blades, Infrared Phys. Technol. 94 (2018) 255–262, https://doi.org/10.1016/j.infrared.2018.09.004.